

# Fault Afterslip and Upper Crustal Relaxation Following the Northridge Earthquake

Andrea Donnellan

Gregory Lyzenga

*Jet Propulsion Laboratory, California Institute of Technology, Pasadena, California*

## Summary

Geodetic observations indicate that significant aseismic deformation occurred following the January 17, 1994 Northridge earthquake. Observations near the earthquake source indicate that afterslip occurred on the rupture plane. In addition, the data strongly suggest viscous relaxation of a 5 km thick soft upper crustal layer or equivalent elastic slip on a shallow low-angle thrust fault in the wedge lying above the hypocenter. The afterslip and relaxation for a two year period following the earthquake result in a moment release of approximately  $1.7 \times 10^{18} \text{ N}\cdot\text{m}$  which is 27% of the mainshock moment release and is equivalent to a  $M_w$  6.3 earthquake. While we expect that the moment release due to the afterslip and relaxation effectively reduce the earthquake hazard, locally, it is not clear to what extent the postseismic deformation loads the surrounding faults or alters the state of stress on those faults.

## Background and Observations

The magnitude 6.7 Northridge earthquake occurred on the morning of January 17, 1994 (1). This thrust earthquake was located in the densely populated San Fernando Valley in Los Angeles County. It ruptured a south-dipping ramp from a hypocentral depth of -20 km in the central part of the valley, breaking upward and northward towards the

mountains to a minimum depth of -5 km (2). The rupture was -18 km in lateral extent and the average slip on the fault was estimated to be about 101–130 cm (3).

Global Positioning System (GPS) data have been collected in the region just to the west of the epicenter of the Northridge earthquake since 1987 as part of a geodetic study of the Ventura basin (4, 5; Figure 1). The basin is marked by an extraordinarily thick sedimentary section (6, 7), which is extensively folded near the surface. East-west striking thrust faults bound the basin and dip away from the central trough (8). The pre-Northridge GPS data indicate rapid shortening of the basin and are best modeled by slip on thrust faults extending into the lower crust (4, 5; the modeled thrust fault systems extended the full 100 km length of the basin and include the Northridge rupture plane).

The last GPS measurements prior to the earthquake were collected in November, 1993. In the one month following the earthquake, the network was reoccupied and two additional stations were established near the source of the earthquake: one at California State University Northridge (CSUN) and another in the Granada Hills just south of the Santa Susana Mountains and near the upper terminus of the rupture plane (LNCH). The stations were reoccupied at approximately 6 month intervals through the summer of 1995. A continuously operating station (OATT) was installed on Oat Mountain near one of the original Ventura basin network monuments. The GPS data were processed using the GIPSY/OASIS 1 I software and JPL precise orbits and clocks (9).

Determination of the post-seismic deformation field is dependent on a clear understanding of the pre-seismic velocities. Any post-seismic transients appear superposed over the background velocity field. For this study we used a velocity field computed for the region that included only GPS geodetic data collected prior to the Northridge earthquake (10). While independent velocity solutions exist for the region (11) these solutions generally include data collected after the earthquake, and while they account for co-seismic offsets, they are potentially biased by post-seismic transients. The velocity differences

between the pre-quake rates and the average post-seismic velocity over the 1.5 years following the mainshock were estimated for all of the stations (Figure 1). Stations TWST, WHIT, LNCH, and CSUN either had poorly determined pre-quake velocities or did not exist prior to the earthquake and therefore their pre-earthquake velocities were interpolated from nearby stations. The pre-earthquake east component of velocity for CATO is probably poorer than suggested by the error ellipse; the east rate component varies substantially between different velocity solutions.

For the present study we assume that any vertical velocities were zero prior to the earthquake, since vertical velocities determined from early campaign-style GPS measurements are of small magnitude and not distinguishable from null motion. In contrast, the vertical components are among the best determined post-seismic motions in the present study (mostly because of their comparatively large amplitude). They indicate uplift over the rupture plane similar in distribution, but smaller than to the co-seismic results (12; Figure 2). The peak measured uplift is 12 cm above the upper edge of the rupture plane. The post-seismic pattern of the horizontal motions is also similar to the co-seismic pattern (Figure 1), with stations to the north and south of the rupture moving toward the rupture plane, and stations east and west moving away from the rupture.

The post-seismic transients decay with time, with most of the motion occurring within the first year after the earthquake (Figure 3). The post-seismic motions can be fit fairly well by an exponential time dependence ( $y = a(1 - \exp(-bt))$ ) with a characteristic decay time in the range 0.8–1.4 years. They can be fit equally well (or perhaps slightly better) by a logarithmic function ( $y = a \ln(t) + b$ ). Exponential decay characterizes relaxation of a Maxwell viscoelastic solid, while fault afterslip may be expected to obey a logarithmic law (13).

## Models

We formulated a series of models in an effort to explain the observed pattern and time history of surface deformation. Forward finite element models and inverse dislocation solutions were employed to examine complementary scenarios of anelastic crustal deformation and elastic afterslip. We begin by eliminating those models that clearly fail to reproduce the observed motions and then proceed to discuss candidate models that are generally consistent with observation.

In the series of finite element models, a viscoelastic rheology is invoked for parts of the crust and upper mantle, in order to accommodate long-term plastic strain during the postseismic and interseismic periods. The baseline model is a simplified two-dimensional layered structure consisting of elastic crust down to a depth of 15 km (based on the approximate lower depth limit of California seismicity; *14*). A viscoelastic lower crust is assumed from 15 km to a Moho depth of 35 km. The rheology of the deepest layers below 35 km does not strongly influence the present results, and is assumed to have a nominal Maxwell rheology roughly approximating the nonlinear flow law of olivine (*15*) and having a relaxation time of 100 years.

The most conventional viscoelastic model of postseismic relaxation simply relies on the flow of lower crustal (and to a lesser degree mantle) material to explain transient deformation. Here, this layer is assigned a Maxwell viscoelastic rheology with a relaxation time of 300 years. This time constant is longer than is typically assumed for southern California models, but it is believed to be appropriate for this region of cool crustal downwelling (*16*) and low crustal heat flow (*17*). While the lower crustal viscosity is not very strongly constrained by geodesy, pre-earthquake strain profiles favor a relatively cold and stiff lower crust in this region (*18*). Such a long characteristic relaxation time is inadequate to explain the kind of short-term transient motions observed after the Northridge earthquake. In addition to predicting the wrong time dependence, lower crustal viscoelastic

relaxation tends to produce motions with amplitude, spatial extent and even sign that are discordant with the observed motions.

Non-Newtonian rheology, in which the effective viscosity (and resulting relaxation time) would be greatly reduced by the coseismic stress increment near the fault, may be invoked as means of explaining rapid transient relaxation. This was achieved in the finite element models by assigning the lower crustal layer a power-law rheology in which strain rate varies as the third power ( $n=3$ ) of the ambient stress. Although such rheological descriptions of crustal rocks maybe derived from laboratory tests (15), the assignment of a specific flow law here is largely empirical. We selected the particular stress-dependent viscosity to provide about a 1 year relaxation time scale for stresses on the order of the coseismic stress drop. In this model, the effective viscosity (and relaxation time) decrease as the square of the crustal stress, so that at typical interseismic strain rates and stresses, the effective Newtonian relaxation time is increased to ~30 years. While in this case the horizontal motions are compatible with the observed motions, the predicted vertical motions have the opposite sense of those observed. These results suggest instead that a model with relaxation in shallow material updip from the rupture zone may be more promising.

We then consider a model in which the sediments in the upper crust are allowed to plastically deform following the earthquake. Such a model seems plausible for the Northridge area because the fault only ruptured to within 5 km of the surface and the region is characterized by soft marine sediments. A model in which a 5 km thick upper sedimentary layer is treated as a viscous material with a relaxation time of 1 year fits the data better than models that allow for afterslip only on the rupture plane.

We investigated the predicted effects of a soft upper crust in an otherwise homogeneous half-space by first running forward models for a two-dimensional thrust fault overlain by a soft upper crust of varying thickness. Subsequently the model surface displacements were inverted for an effective elastic fault source. In each of these models

the effective fault is located above the actual fault plane in the hanging wall block, with the effects more pronounced for a thicker soft layer. The sense and amount of offset from the earthquake rupture plane are consistent with the shift apparent in the coseismic GPS solutions (12).

Our preferred model incorporates roughly equal contributions from shallow viscous relaxation (represented by a shallow hanging wall thrust fault), and afterslip on the rupture plane (Figure 4). The model presented here was obtained by excluding site JPLM from the fit because it is a large outlier (see below); the resulting model explains the combined horizontal and vertical displacements with a fit  $\chi^2/\text{dof} \approx 0.88$  and 22 degrees of freedom (19). Thirty-five inversion trials were performed to test the sensitivity of the model using both one and two fault models, and differing initial constraints and free parameters.

The preferred model predicts a dual maximum in the surface uplift pattern (Figure 5), although the available data cannot corroborate this in detail. The best competing models, which also require two faults, one on the rupture plane and one above, feature a single composite uplift feature, however in this second domain the  $\chi^2/\text{dof}$  is consistently worse (typically  $>1.6$ ). Among the robust features of the model is the requirement of significant and comparable amounts of moment release in (1) the mainshock rupture plane and (2) the sedimentary hanging wall block, This is furthermore consistent with aftershock patterns, which both outline the rupture plane and form a diffuse distribution in the upper crustal wedge (20). The estimated along-strike length of both dislocations is about 20 km. In the absence of higher resolution observations (from, for example, radar interferometry or leveling), we can only conclude that the current model adequately explains most near-field displacements, but may or may not accurately describe the detailed configuration of motions nearest the rupture. Furthermore, the model does not explain the farther field observations. Continued observations across the Ventura basin will clarify the response of

the basin and surrounding faults to the Northridge earthquake. Unfortunately, there are not enough detailed observations near JPL to explain the motion at that station.

The largest unmodeled horizontal residual velocity occurs in the far-field at the station JPLM (Figure 1; the model prediction is nearly zero in length). Our model describes the general characteristics of the near-source effects of the earthquake, but other processes must control the farther field motions, particularly the transient motion at JPLM, which is the specific subject of an accompanying paper (this issue). Other large residuals are found at WHIT and TWST, although, both stations have potentially inaccurate pre-Northridge velocities.

## **Implications**

These observations indicate that different processes dominate before and after the earthquake. Pre-Northridge geodetic observations are best explained by relaxation of a stiff viscoelastic lower crust (18). Relaxation of the lower crust causes vertical motions that are opposite in sense from those observed in the postseismic period; further, the predicted rates of motion from this mechanism are an order of magnitude smaller than those observed. Therefore, the presence of a stiff viscoelastic lower crust is not inconsistent with the post-earthquake observations, but is not the process controlling the post-seismic deformation.

Conversely, the post-seismic mechanisms that we propose here do not apparently play a significant role late in the earthquake cycle. Our observations indicate a post-seismic decay time constant of about 1 year, implying that essentially all of the shallow post-seismic deformation should have occurred within 5 years after the earthquake. Our relaxation models assume a simple exponential decay rate and only additional observations will verify if this is appropriate. Additional observations will also indicate how other faults near Northridge and the Ventura basin have been affected by the Northridge earthquake.

The post-seismic moment release over the two-year period following the earthquake is about  $1.7 \times 10^{18} \text{ N}\cdot\text{m}$  or 27% that of the mainshock moment release. This follows from the inference of about 13 cm/yr of post-seismic slip occurring on the upper part of the rupture plane and about 15 cm/yr of equivalent displacement occurring through deformation of the sedimentary layer in the upper crust in the two years following the earthquake. Deformation of a soft sediment layer most likely would occur through folding, and folds are pervasive in the Northridge region (8).

Inversions for co-seismic fault slip have been carried out using strong motion, teleseismic, and geodetic data (3). Those inversions that include geodetic data predict a 10-30% larger average slip for the Northridge earthquake than those that include only seismic data. Observations of postseismic release on the order of 10-20% of coseismic are not unusual following other earthquakes of comparable and larger size (21–25). It is possible that the geodetic data (particularly the leveling data), which were collected up to 8 months after the earthquake, reflect post-seismic as well as co-seismic motions, which would result in a higher estimate of slip than from a solution using only seismic data. The slip discrepancy for inversions that include the leveling data is generally consistent with the post-seismic slip that we infer from the GPS observations.

These model results also suggest that a plastic upper crustal rheology has consequences observable in the (nominally) coseismic geodetic data. Published inversions for coseismic fault slip constrain the modeled fault to coincide with the aftershock zone (3). However, when the GPS geodetic data are inverted for fault slip, location and orientation in an isotropic elastic half-space, the preferred fault plane is located 2--3 km above the aftershock zone (12). Since these geodetic data were acquired over a period of weeks following the main shock, they are likely to be partially contaminated by postseismic deformation.

The post-seismic mechanisms that we propose may explain why the upper portion of the crust can be well described by thin-skinned tectonic models, while the major recent earthquakes tend to rupture on moderately steeply dipping faults extending from the lower crust as described by thick-skinned tectonic models. It may be that thick-skinned processes dominate for the moderate to large earthquakes and that thin-skinned processes occur following these events as a means of redistributing stress. Thin-skinned tectonics are described by low angle faults that terminate in folds (26). The relaxation of the soft upper crust may be a proxy for folding of the sediments and bedding plane faults may form where the stress concentrations are greatest following earthquakes. Our best fit model requires relaxation (e.g. folding) of the upper crust and/or a shallow low-angle fault (perhaps a bedding plane fault) located above the main rupture plane, as well as some afterslip on the main rupture plane.

Based on the inferred decay rate, about 30% of the mainshock moment release is expected to accumulate quietly in the years following the earthquake. This is the moment equivalent of a magnitude 6.3 earthquake. If aseismic deformation commonly occurs following moderate to large earthquakes in southern California, earthquake potential and hazard estimated on the basis of regional strain accumulation may require reassessment. We account for aseismic deformation in the near-field of a moderate earthquake. Other aseismic processes may occur, which would further reduce the percentage of seismic moment release in southern California. The 30% near-field reduction of seismic moment release is not large enough alone to rule out the possibility of either more frequent moderate earthquakes than historically observed or larger  $M_w$  7.1 –7.5 earthquakes in the Los Angeles region (27).

## **References and notes**

1. Jones, L., K. Aki, M. Celebi, A. Donnellan, J. Hall, R. Harris, F. Hauksson, T. Heaton, S. Hough, K. Hudnut, K. Hutton, M. Johnston, W. Joyner, H.

- Kanamori, G. Marshall, A. Michael, J. Mori, M. Murray, D. Ponti, P. Reasenberg, D. Schwartz, L. Seeber, A. Shakal, R. Simpson, H. Thio, M. Todorovska, M. Trifunic, D. Wald, and M. L. Zobak, *Science*, 266, 389-397 (1994).
2. Hauksson, E., L.M. Jones, K. Hutton, *J.Geophys. Res.*, 100 , 12,335–12,355 (1995).
  3. Wald, D. J., T.H. Heaton, K.W. Hudnut, *Bull.Seism. Soc. Am.*, 86, S49–S70 (1996). Alternative slip distribution models such as given in (11) suggest different fault area and mean slip, but similar overall moment.
  4. Donnellan, A., B. H. Hager, and R. W. King, *Nature*, 366, 333-336 (1993).
  5. Donnellan, A., B. H. Hager, R. W. King, and T. A. Herring, *J.Geophys. Res.*, 98, 21,727-21,739 (1993).
  6. Luyendyk, B.P. and J. S. Hornafius, in *Cenozoic Basin Development of Coastal California*, 6, R. V. Ingersoll and W. G. Ernst, Eds. (Prentice Hall, Inc., Englewoods Cliffs, NJ, 1987), pp. 259-283.
  7. Norris, R.M. and R.W. Webb, *Geology of California*, (John Wiley & Sons, Inc., New York, 2nd cd., 1990).
  8. Yeats, R. S., *J. Geophys. Res.*, 88, 569–583 (1983).
  9. Zumberge, J. F., M.B.Heflin, D.C. Jefferson, M.M. Watkins, and F.H. Webb, Precise point positioning for the efficient and robust analysis of GPS data from large networks, *J. Geophys. Res.*, in press.
  10. D. Dong, unpublished results.
  11. For example, the Southern California Earthquake Center (SCEC) has released a regional velocity model which is accessible via the the Internet at URL

- <http://minotaur.ess.ucla.edu/velmap/welcome.shtml>. Shen, Z., D.D. Jackson, and B.X. Ge, *J.Geophys.Res.*, 101, 27,957-27,980 (1996).
12. Hudnut, K. W. , Z. Shen, M. Murray, S. McClusky, R. King, T. Herring, B. Hager, Y. Feng, P. Fang, A. Donnellan and Y. Bock, *Bull. Seism. Soc. Am.*, 86, S 19–S36 (1996).
  13. Marone, C. J., C.H.Scholz, R. Bilham, *J.Geophys. Res.*, 96, 8441--8452 (1991).
  14. Webb, T.H. and H. Kanamori, *Bull. Seism. Soc. Am.*, 75, 737-757 (1975).
  15. Poirier, J. P., in *Mineral physics and crystallography: a handbook of physical constants*, T. J. Ahrens, Ed. (American Geophysical Union, Washington, DC, 1995), pp. 237–247.
  16. Humphreys, E. D., R.W. Clayton, *J.Geophys. Res.*, 95, 19725-19746 (1990).
  17. DeRito, R.F, A.H. Lachenbruch, T.H. Moses, and R.J. Munroe, *J.Geophys. Res.*, 94, 681-699 (1989).
  18. Hager, B. H., G. A. Lyzenga, and A. Donnellan, in preparation.
  19. The estimated uncertainties in velocity have been scaled such that  $\chi^2/\text{dof}=1$ .
  20. Mori, J., D.J. Wald, and R.L. Wesson, *Geophys. Res. Lett.*, 22, 1033--1036 (1995).
  21. Argus, D. F., G.A. Lyzenga, Site velocities before and after the Loma Prieta and Gulf of Alaska earthquakes determined from VLBI, *Geophys. Res. Lett.*, 21, 333–336 (1994).
  22. Barrientos, S. E., G. Plafker, E. Lorca, Post-seismic coastal uplift in southern Chile, *Geophys. Res. Lett.*, 19, 701–704 (1992).
  23. Savage, J. C., and M. Lisowski, Changes in long-term extension rates associated with the Morgan Hill and Lorna Prieta earthquakes in California, *Geophys. Res. Lett.*, 22,759-762 (1995).

24. Lisowski, M., W.H. Prescott, J.C. Savage, and M.J. Johnston, Geodetic estimate of co-seismic slip during the 1989 Loma Prieta, California, earthquake, *Geophys. Res. Lett.*, 17, 1437-1440 (1990).
25. Shen, Z. K., D.D. Jackson, Y.J. Feng, M. Cline, M. Kim, P. Fang, and Y. Bock, Post-seismic deformation following the Landers earthquake, California, 28 June 1992, *Bull. Seism. Soc. Am.*, 84, 780-791 (1994).
26. Suppe, J. and D.A. Medwedeff, *Eclogae, Geol. Helv.*, 83, 409–454 (1990).
27. DoIan, J. F., K. Sieh, T.K. Rockwell, R.S. Yeats, J. Shaw, J. Suppe, G.J. Huftile, and E.M. Gath, *Science*, 267, 199-205 (1995).
28. We gratefully acknowledge the invaluable assistance of M. B. Heflin, M. Watkins, D. Jefferson, F. Webb, D. Dong and W. Panero in the analysis and modeling of the geodetic data. We are grateful for the help of D. Darger, M. Glasscoe, K. Hurst, G. Franklin and M. Smith in the field acquisition of data. This work was carried out at the Jet Propulsion Laboratory, California Institute of Technology, under contract with NASA. Support was provided by the U.S. Geological Survey and National Science Foundation through the National Earthquake Hazards Reduction Program (NEHRP) and the Southern California Earthquake Center (SCEC).

## Figures

Figure 1: Post-Northridge GPS network, observed residual post-seismic velocities (light vectors) averaged for 1.5 years after the Northridge earthquake, and modeled velocities (heavy vectors). Error ellipses represent 90% confidence. The square patch shows the approximate projection of the rupture plane onto the surface. The epicenter of the earthquake is marked by the star. Dashed and dotted lines mark major and minor fault traces.

Figure 2: North-south profile of observed and modeled vertical velocities for the 1.5 year period following the mainshock. The 2D finite element model show the results from upper crustal relaxation following an earthquake on a 40° dipping plane and the 2D dislocation model shows the surface velocities for a dislocation simulating upper crustal folding, faulting, and flow.

Figure 3: Vertical time series for the station Lynch (LNCH) located in the Granada Hills near the upper part of the mainshock rupture. plane.

Figure 4: Cartoon of preferred postseismic processes that occurred in the 1–2 year period following the Northridge earthquake including relaxation of a soft upper crustal layer and slip on the main rupture plane. The upper fault with a lower dip angle yields displacements similar to those due to relaxation of a soft upper layer following a Northridge type event,

Figure 5: Calculated horizontal (vector field) and vertical velocities (color contours) for the preferred post-seismic deformation model in the region encompassing the mainshock rupture. Nearfield station locations are shown by the dots and the epicenter of the earthquake is marked by the star.

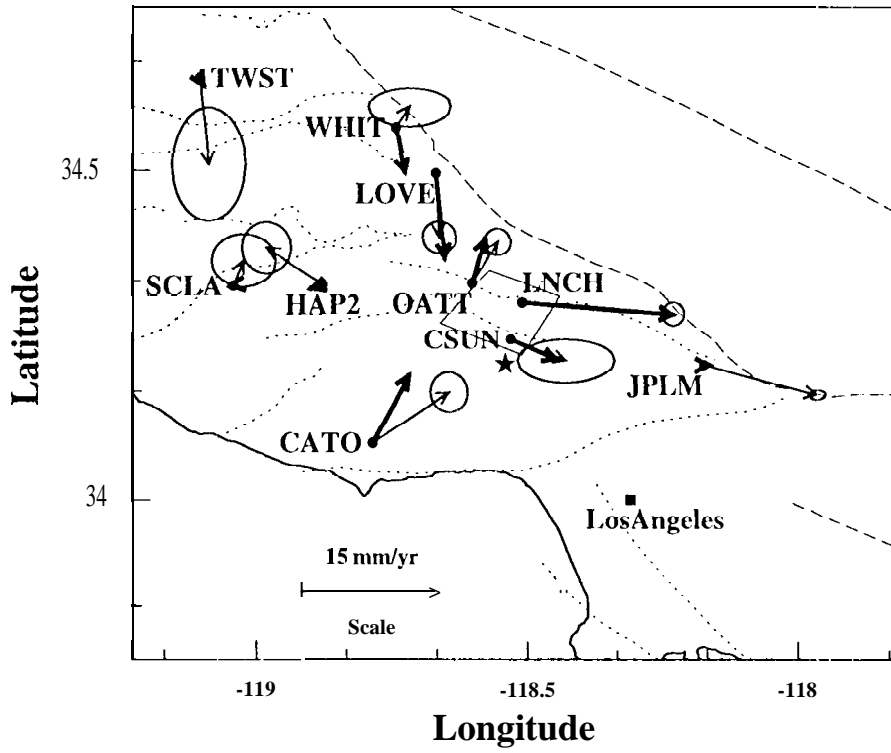


Figure 1

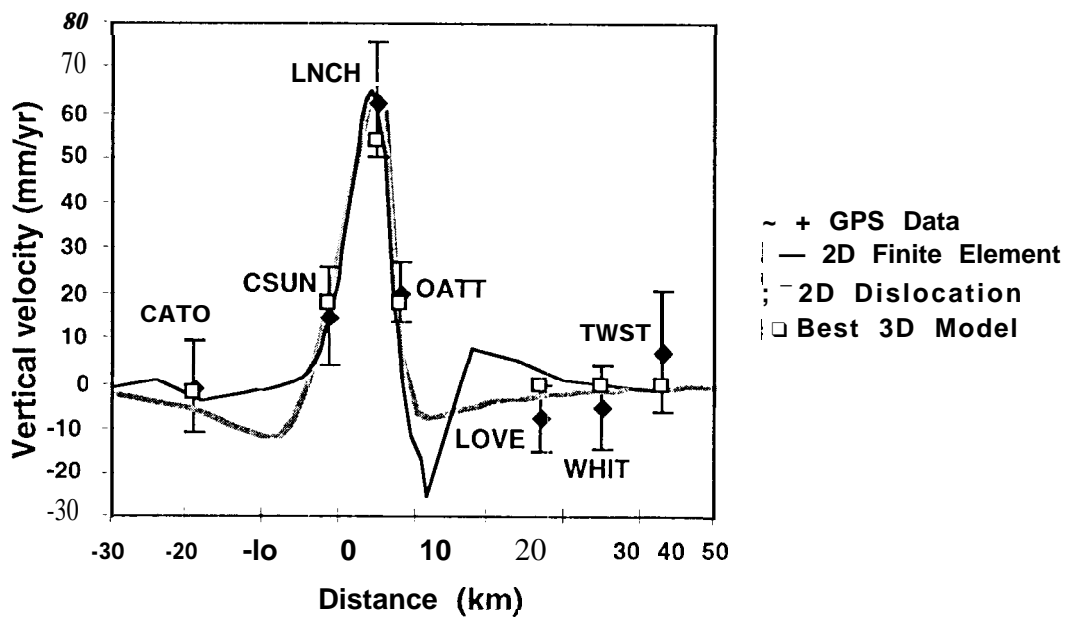


Figure 2

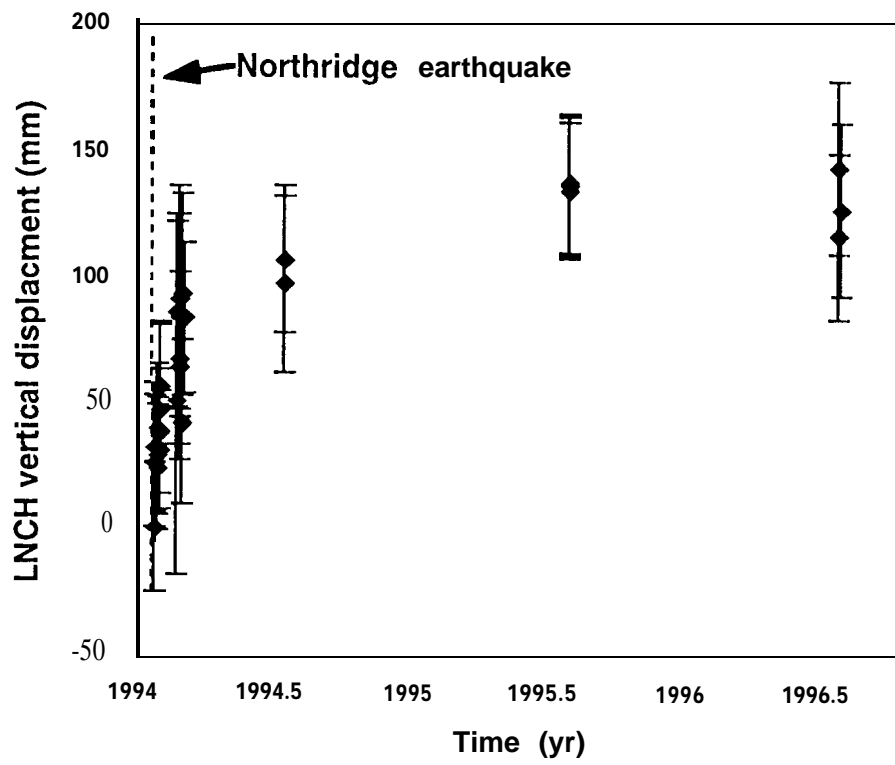


Figure 3

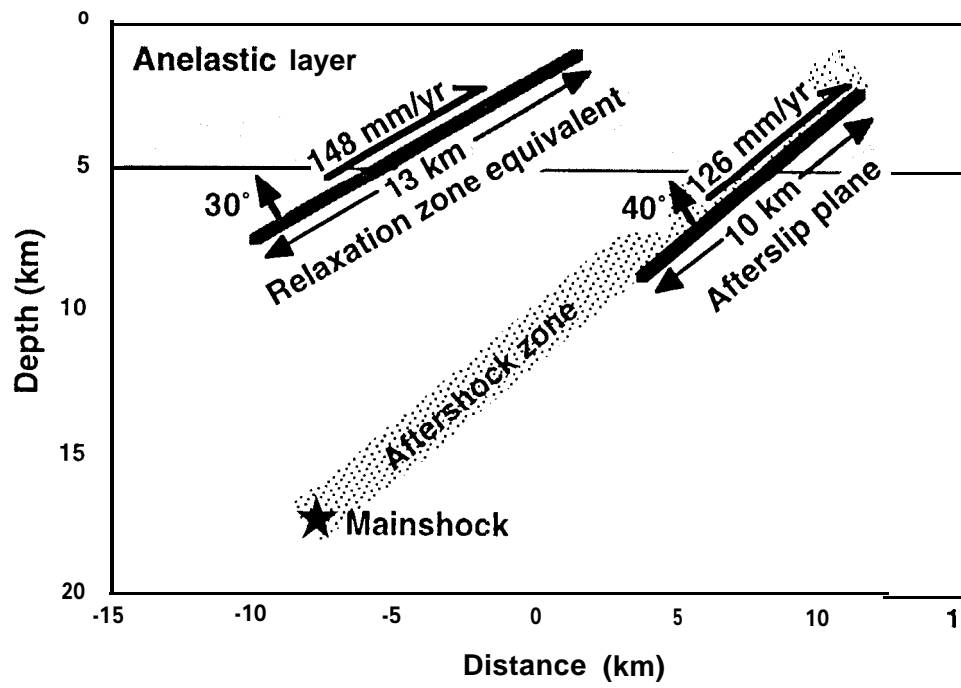
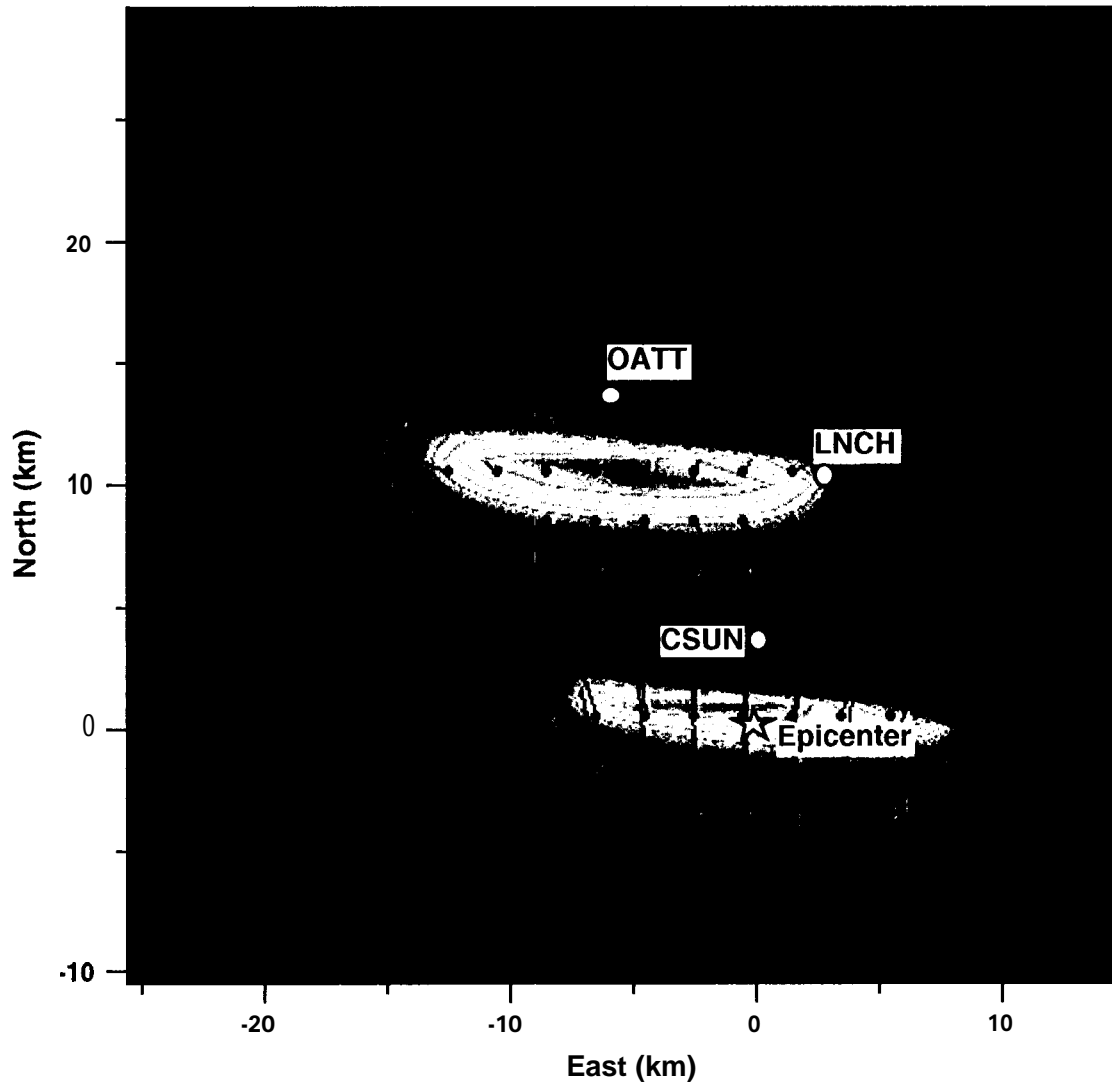


Figure 4



Vertical velocity (mm/yr)

50 mm/yr

Horizontal velocity

1 figure S